Appl. Phys. B 87, 523–530 (2007)
DOI: 10.1007/s00340-007-2593-y

Applied Physics B
Lasers and Optics

L. PERSSON[1,✉]
F. ANDERSSON[2]
M. ANDERSSON[1]
S. SVANBERG[1]

Approach to optical interference fringes reduction in diode laser absorption spectroscopy

[1] Division of Atomic Physics, Lund University, P.O. Box 118, 22100 Lund, Sweden
[2] Centre for Mathematical Sciences, Lund University, P.O. Box 118, 22100 Lund, Sweden

Received: 6 October 2006/Revised version: 18 January 2007
Published online: 24 March 2007 • © Springer-Verlag 2007

ABSTRACT The advantage of a new scheme for balanced detection has been investigated to reduce the influence of optical interference fringes when performing diode laser gas absorption spectroscopy employing lock-in amplifiers and pigtailed lasers. The influence of the fringes has been reduced by comparing the lock-in 2 f signal due to the gas sample with that of a reference beam. The frequency regions outside the absorption feature have been used to obtain information on the interference fringe impact on the signal of interest. We have demonstrated an efficient way to reduce the influence of such fringes by employing this technique combined with non-linear signal processing methods. The different steps of the algorithm are presented. In the experimental arrangement presented, a reduction of the optical interference fringes by about 10 times is achieved, as demonstrated in measurements on molecular oxygen around 761 nm. The new technique is compared with an analog technique for balanced detection and certain advantages of the computer algorithm are pointed out. In particular, the emerging field of gas spectroscopy in scattering solid media strongly benefits from the technique presented.

PACS 42.55.Px; 39.30.+w; 42.25.Hz

1 Introduction

Diode laser absorption spectroscopy is increasingly used for monitoring gases in environmental, biological, and medical contexts [1, 2]. In many applications the gas concentration is in the sub-ppm (part-per-million) range, i.e. when dealing with trace-gas detection. As a result, measurements are heavily influenced by noise, interfering signals, and drifts. Different modulation techniques have been introduced to reduce the detrimental effects of noise. These techniques are based on imposing a high-frequency modulation signal to the injection current of the light source. The signal is then detected using phase-sensitive techniques at some harmonic of the modulation frequency [2, 3]. Even though such techniques may cancel out the effect of excess laser noise and reduce background fluctuations, they do not compensate for optical interference fringes. Seldom discussed in the literature, interference fringes constitute in practice the real limitation in low-level gas analysis. Interference fringes appear in light being partially reflected at optical surfaces. A light beam vertically impinging from air onto a common optical material of refraction index n undergoes a fractional reflection of $R = ((n-1)/(n+1))^2 \approx 4\%$. The reflected light from different surfaces can interfere causing a complex pattern intensity Fabry–Pérot fringes. Even if surfaces are anti-reflection coated or tilted, residual intensity variations easily occur on the per mille intensity scale. Clearly, this is of no concern for substantial absorption signals, but can become critical in the case of very weak absorptions, for which the sensitive modulation techniques have been developed.

Interference fringes can originate from various parts of the optical path between the laser and the detector. The fringes may obscure weak absorption signals if the free spectral range of the optical fringes is in the same order as the line width of the absorption signal, the half width of the fringes being also in this range due to the low finesse ($I_{\max}/I_{\min} = ((1+R)/(1-R))^2 \approx 1.2$ for $R = 4\%$) [4]. Several techniques have been introduced over the years to reduce the influence of optical interference fringes. Specific examples include signal averaging, mechanical vibration, and balanced detection [5–8]. Mechanical vibrations, however, are not applicable when using a fixed-optical-surface pigtailed laser, which is attractive for different reasons to be further discussed.

Balanced detection is commonly used to cancel out laser intensity fluctuations such as optical interference fringes. The general idea is to split the initial laser beam into two, where one beam, called the sample beam, passes through the sample, and the other beam, called the reference beam, goes directly to a detector. The analog balanced detection techniques can be divided into two groups. The first is based on subtraction of small currents (μA range) from photodiodes [9, 10], while the second is based on subtraction of voltage signals created by two identical transimpedance amplifiers [11–14]. Both techniques commonly use a feedback loop in order to minimize the difference between the detector signals. Subtraction of current signals should give better performance but requires careful design and closely mounted matched detectors. In practice this may be hard to implement and therefore solutions based on subtraction of signals from transimpedance amplifiers have been introduced. While these methods clearly improve the signal recovery they have certain drawbacks. The two detectors should be placed close to each other, in order to minimize additional noise and to optimize performance. The analog balanced detection method also frequently assumes

✉ Fax: +46-46-222-4250, E-mail: linda.persson@fysik.lth.se

that the reference beam power is larger than the sample beam power, as well as that matched detectors and matched transimpedance amplifiers are used. In many applications these conditions are not feasible, as discussed below.

Historically, diode laser spectroscopy has been performed on well-defined atmospheric beam paths, frequently in absorption cells, where the conditions with regard to the geometry and transmission are very stable (see [14] for an extensive review of molecular oxygen diode laser spectroscopy performed under such conditions). Then the cell can be evacuated allowing a subtraction of persistent fringes. In contrast, in applications recently developed in our group [15–19], the gas cell is replaced by a test sample that attenuates and scatters light differently during the measurements or on a day to day basis, which puts new demands on the detection- and signal-processing systems. In [17], wood-drying processes were studied by spectroscopic measurement of oxygen and water vapor. It turned out that the sample beam intensity varied by a factor of 10–100 depending on the water content. Spectroscopic measurements on pharmaceutical tablets put similar demands due to the differences of thickness and density of the tablets [18]. Further applications resulting in similar demands are measurements for medical diagnostics. In [19], spectroscopic measurements on human maxillary sinuses were described. It turned out that the intensity of the sample beam varied by a factor of 20 depending on the person that was studied even if the measurement procedure was the same. Thus, it is not enough to calibrate the system for a limited intensity range or use commonly known techniques to suppress non-linear disturbances, fringes, etc. The situations with sample beam intensity varying by several orders of magnitude depending on the state of the test sample is vastly different from the conventional trace-gas measurements in an absorption cell.

We largely use pigtailed lasers since it is not practical to measure on solid test samples with ordinary lasers. Backscattered light from the sample that enters the laser, fringes due to fibre coupling based on lenses, and handling laser heads close to a test sample at measurement all can be problematic. The present paper focuses on applications based on pigtailed lasers which are easy to implement in portable measurement systems for a variety of spectroscopic studies.

In the present paper, we describe a specific way of using software-based balanced detection to remove optical interference fringes in strongly varying measurement situations as described above. Our approach is based on using parts of the recorded signals falling in the frequency range outside the absorption region in order to estimate imperfections of the measurement system. In the reference beam, unaffected by gas absorption, fringe structures are also recorded in the frequency region of the gas absorption. The regions outside the absorption can be used to estimate the fringe contribution to the gas signal. In addition, the algorithm presented compensates for possible non-linear effects in the response of the two different detection arms as well as different offsets. This method can be applied to any system and be combined with other customary techniques such as mechanical vibrations to further reduce fringes not related to the common light path.

In Sect. 2 the experimental arrangements for this study are described. The different artifacts that occur in typical diode laser absorption spectroscopy experiments are then discussed together with an explanation of the presented software-based method and a previously discussed analog method for achieving balanced detection. The procedure to evaluate the gas content from the balanced-detection signals is then discussed. Results from both the software-based balanced detection and the balanced detection achieved by the electronic circuit are then shown and discussed. Finally, conclusions are drawn.

2 Experimental arrangements

Schematic drawings of the experimental arrangements used in the software-based and the analog balanced detection approaches are shown in Fig. 1. Common for both cases (Fig. 1a), a single-mode fibre-pigtailed thermoelectrically cooled DFB laser diode (Nanoplus, Germany) was used as a light source. The laser delivered about 4 mW at around 760 nm, where the molecular oxygen A-band is located. The wavelength of the light was tuned across the R11Q12 absorption line by supplying a 4 Hz saw-tooth ramp to the laser driver current. A 10 kHz sine wave was also superimposed on the laser driver current in a wavelength-modulation scheme to achieve sensitive detection.

The light was split 90%/10% with a single-mode fibre-coupled beam splitter (Laser2000, Sweden) with an insertion loss of about 5%. The fibre carrying about 10% of the light was directly guided to a silicon detector (UDT 10DP/SB) via an attenuation filter ($\times 10$). Thus, about 0.035 mW light enters the detector, which was connected to a transimpedance amplifier. The other fibre carrying about 90% of the output from the laser was connected to a collimating lens package (Thorlabs CFC-5-760). The light then travels over a certain air distance, or an absorbing and scattering medium, before being detected with a second identical silicon detector or a photomultiplier tube (PMT), which is connected to an identical transimpedance amplifier as the one used for the reference detector. An attenuation filter was mounted in between the fibre and the detector for the case of a non-scattering sample. The collimating package was mounted on a z-translator providing variable air distances. For the amplification, Hamamatsu C7319 units were available and used.

2.1 *Setup for software-based balanced detection*

In the left-hand part of Fig. 1b the arrangement to perform software-based balanced detection is shown. The reference signal was sent to an oscilloscope via a lock-in amplifier (EG&G Princeton Applied Research 5209), where the 2 f signal was recorded. This signal will be referred to as the reference signal. The signal from the sample detector was split into two parts; one part directly was connected to the oscilloscope (referred to as the direct signal) while the second part was sent via a second lock-in amplifier (EG&G Princeton Applied Research 5209) before being connected to the oscilloscope where the 2 f signal was recorded. This signal will be referred to as the sample signal.

2.2 *Setup for analog balanced detection*

In order to test the performance of an auto balanced detection approach, based on differential transimpedance am-

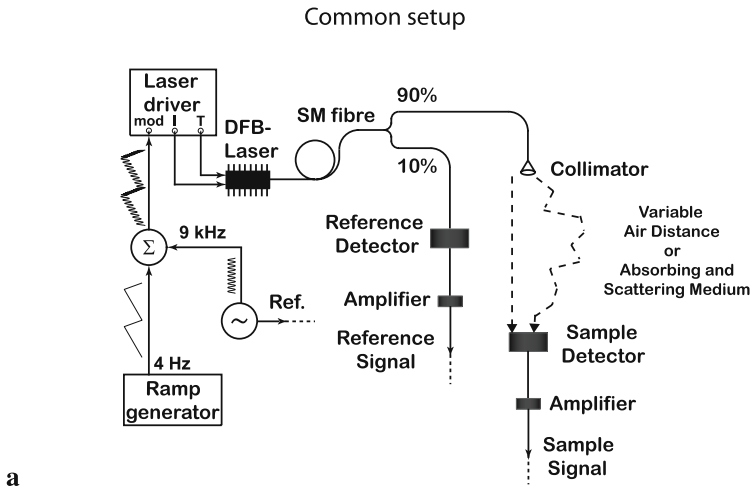

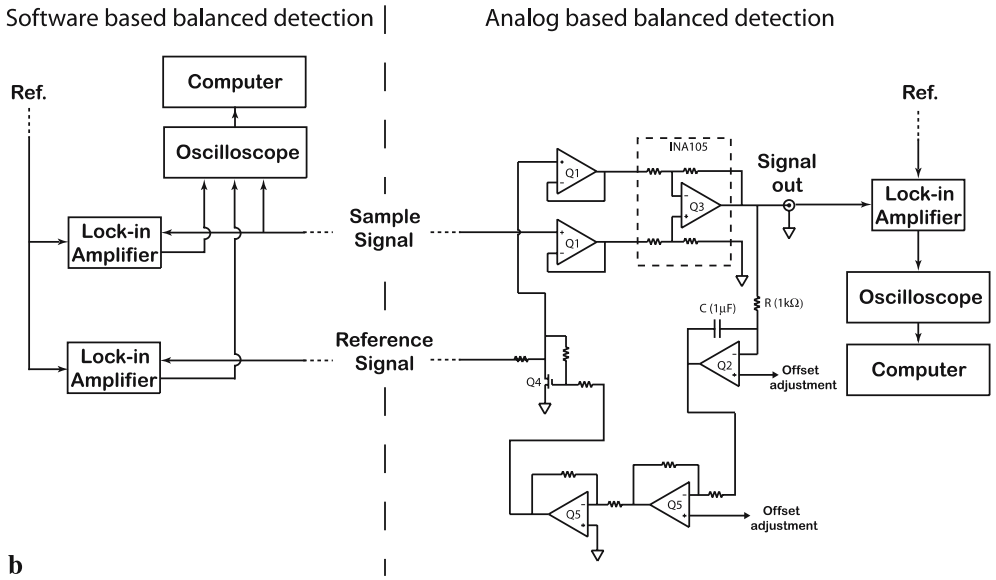

FIGURE 1 (**a**) Schematic drawing of experimental arrangement for diode laser gas absorption spectroscopy providing balanced detection. (**b**) In the *left-hand part* the arrangement for software-based balanced detection is shown and in the *right-hand part* the arrangement for analog balanced detection is shown [11]. The following components were used in the device: Q1 and Q5 – OP470 low-noise op-amp, Q2 – LF356 low-noise op-amp, Q3 – INA105 unity-gain differential amplifier, and Q4 – 2N5457 MOSFET

plification, we implemented an electronic cancellation device, according to [11], shown to the right in Fig. 1b. The sample signal is buffered by Q1 and fed into a unity-gain differential amplifier (INA105). The reference signal was connected to the unity-gain differential amplifier via a field-effect transistor (Q4). A feedback loop consisting of Q2 and Q5 controls the input level of Q4 (attenuation factor), trying to minimize the output of the differential amplifier. Thus, the output of the differential amplifier is proportional to $U_{\text{sample}} - U_{\text{reference}}$. The time constant of the feedback loop ($t = 0.001$ s) is set by the 1 kΩ resistor and the 1 μF capacitor mounted closely to Q2. The output of the noise cancellation circuit was led into a lock-in amplifier of the same type as used in the software-based balanced detection scheme, and the 2 f signal was recorded on an oscilloscope.

3 Data analysis

In order to achieve optimal signal retrieval for weak gas absorption signals we need to handle (a) interference fringes, (b) laser intensity noise, (c) non-linear detector response, and (d) different zero detector offsets.

Fringes mimicking real signals are most critical. They can be eliminated by studying spectral regions outside the expected absorption imprint. This could in principle be done in an exact way from the reference signal if the detection channels (detectors, amplifiers, and lock-ins) were identical, linear, and with a correct zero level. Since this might not be the case – Fig. 2 – the differential behavior between the two signals is described by a set of parameters corresponding to linear and non-linear phenomena, as discussed below.

3.1 *Software-based method for non-linear artifact suppression*

As mentioned above, two outputs from two detectors are measured; one detecting the light which has traveled over the gaseous sample to be analyzed and one measuring the reference light level. We will here denote the sample signal $p_{\text{samp}}(\nu)$ and the reference signal $p_{\text{ref}}(\nu)$. Ideally, $p_{\text{samp}}(\nu)$ and $p_{\text{ref}}(\nu)$ should be identical for ν-values outside the region of oxygen absorption. Hence, by considering the difference between the two signals we can determine the amount of oxygen in the measurement sample, since only effects of oxygen absorption should remain. The difference between the sample

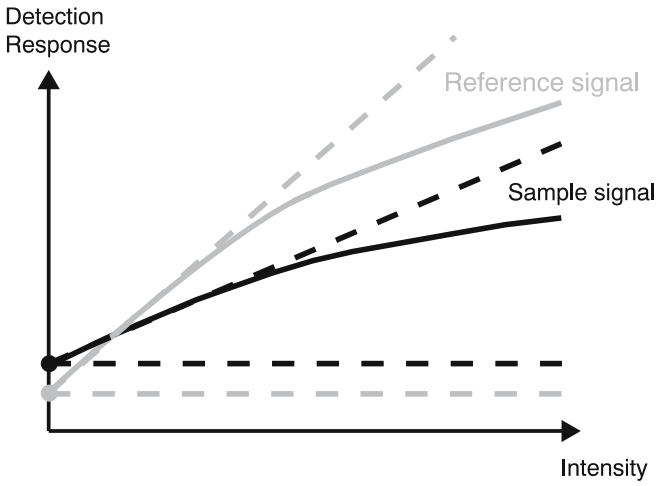

FIGURE 2 Schematic drawing of imperfections in detection arm response (heavily exaggerated)

signal and the reference signal will thus give us the balanced-detection signal, which we will denote $p_{\mathrm{bds}}(\nu)$. However, there are several practical measurement effects that need to be suppressed before constructing the balanced-detection signal.

Let $w(\nu)$ be a window function that vanishes in the neighborhood of the oxygen absorption region, and goes smoothly to 1 outside the region. We assume that data are sampled at points $\nu = \{\nu_j\}$, and introduce column vectors $\mathsf{p}_{\mathrm{samp}}$, $\mathsf{p}_{\mathrm{ref}}$, and $\mathsf{p}_{\mathrm{bds}}$, containing samplings of p_{samp}, p_{ref}, and p_{bds} at $\{\nu_j\}$, respectively. Furthermore, let W be a diagonal matrix with the values of $w(\nu_j)$ as entries. In the case of no difference in offset or in amplification, one would expect that

$$p_{\mathrm{samp}}(\nu)w(\nu) \approx p_{\mathrm{ref}}(\nu)w(\nu)\,. \tag{1}$$

However, due to imperfections of the measurement system, effects from various components bring degradation of the processing. This can be accounted for by considering non-linear effects and different background offsets in the two detectors and the downstream processing. We account for the effects by estimating their impact outside the oxygen absorption region. We expect deviations from (1) due to the effects mentioned above. Hence, we assume that

$$p_{\mathrm{samp}}(\nu)w(\nu) \approx \Big((l_0 + l_1\{\nu-\nu_0\})\,p_{\mathrm{ref}}(\nu) + k_0 + k_1\{\nu-\nu_0\} + k_2\left\{(\nu-\nu_0)^2\right\}\Big)w(\nu)\,. \tag{2}$$

The constants introduced have the following interpretation:

- l_0: Amplification compensation
- l_1: Non-linear response compensation
- k_0: Background offset compensation
- k_1: Intensity-dependent laser stray-light compensation
- k_2: Residual non-linear intensity compensation

all of which are due to the differential behaviors of the two individual detectors and imperfections in the subsequent signal handling.

We can thus estimate the parameters

$$\boldsymbol{h} = \left(l_0\, l_1\, k_0\, k_1\, k_2\right)^{\mathrm{T}}$$

by minimizing the residual of the matrix equation ($\mathsf{1}$ is the column vector containing 1 as elements)

$$\begin{aligned}\boldsymbol{W}\boldsymbol{p}_{\mathrm{samp}} &\approx \boldsymbol{W}\Big(\boldsymbol{p}_{\mathrm{ref}}\{\nu-\nu_0\}\circ\boldsymbol{p}_{\mathrm{ref}}\mathsf{1}\{\nu_j-\nu_0\}\left\{(\nu_j-\nu_0)^2\right\}\Big)\boldsymbol{h}\\ &= \boldsymbol{W}\,\boldsymbol{A}\,\boldsymbol{h}\,,\end{aligned} \tag{3}$$

where ν_0 is the center frequency and where $\circ$ denotes the Hadamard product [20]. Note that (3) is largely overdetermined.

We solve (3) in a (weighted) least-squares sense by forming and solving the normal equations:

$$\mathsf{h} = (\mathsf{A}^{\mathrm{T}}\boldsymbol{W}\mathsf{A})^{-1}\,\mathsf{A}^{\mathrm{T}}\,\boldsymbol{W}\,\mathsf{p}_{\mathrm{samp}}\,.$$

With these $\boldsymbol{h}$-parameters at hand, we define the balanced-detection signal as

$$\mathsf{p}_{\mathrm{bds}} = \mathsf{p}_{\mathrm{samp}} - \big((l_0 + l_1\{\nu-\nu_0\})\mathsf{p}_{\mathrm{ref}} + k_0 + k_1\{\nu-\nu_0\} + k_2\{(\nu-\nu_0)^2\}\big)\,. \tag{4}$$

3.2 *Standard analog artifact suppression*

The analog balanced detection device, based on [11], is in principle a PI controller (integrator with a proportional gain) that adjusts the attenuation of the signal from the reference detector by changing the dynamic resistance of a field-effect transistor (FET). The aim is to minimize the output level of the device and thus suppress low-frequency noise caused by the laser, detector, and fringes. The time constant of the feedback loop is set by two components (C and R in Fig. 1b to the right) and is on the order of 1 ms. Thus, the feedback loop is not affected by the 2 f signal at 20 kHz that is transferred more or less without any distortion. An additional advantage is that the need for lock-in amplifiers with high dynamic range has decreased due to lower signal amplitudes in the low-frequency range.

3.3 *Gas content evaluation*

The gas concentration is evaluated using the Beer–Lambert law stating that

$$I(\lambda) = I_0(\lambda)\mathrm{e}^{-\sigma(\lambda)cL}\,,$$

where $I_0(\lambda)$ is the initial intensity and $I(\lambda)$ is the intensity of the light that has traveled a distance L over a sample with the gas concentration c and the absorption cross section $\sigma(\lambda)$ [4]. Beer–Lambert's law also states that for low absorptions the fractional absorption is proportional to the concentration and the optical path length. Therefore, the balanced-detection signal must be normalized to the amount of light reaching the detector (direct signal). The amplitude of the balanced-detection signal is proportional to the gas content in the sample and is therefore the parameter of central interest in the gas analysis.

When starting a measurement, an ideal experimental absorption profile, $p_{\mathrm{i}}(\nu)$, is first measured where the noise is much smaller than the detected oxygen signal. This signal is obtained by measuring over an air distance of several meters. Once a clean balanced-detection signal is obtained, we can

match it against our computed $p_{\mathrm{bds}}(\nu)$. In the matching process, we compensate for drifts in the frequency scale. Thus, we match the balanced-detection signal against the ideal function with regard to both location and amplitude. This is done by mimicking an autocorrelation function; we convolve $p_{\mathrm{bds}}(\nu)$ with $p_{\mathrm{i}}(\nu)$ and detect the resulting peak position, denoted ν_s. Once the peak position is known, we repeat a similar approach as for the construction of the balanced-detection signal with the algorithm; we form

$$(1-\boldsymbol{W})\,p_{\mathrm{i}} = (1-\boldsymbol{W})\left(p_{\mathrm{bds}}1\right)m = \boldsymbol{W}\,B\,m\,, \tag{5}$$

and solve it for parameters m by forming and processing the corresponding normal equations. The global intensity parameter is then estimated (peak-to-peak value of the fit), which corresponds to the gas content after calibration.

4 Results and discussion

Several measurements were performed with different added air distances to investigate the performance of the implemented software-based balanced detection method. To investigate the influence of the different components in $\boldsymbol{h}$, (3) was solved with different $\boldsymbol{h}$-parameter combinations. Figure 3a shows signals obtained during measurements with an air distance of about 10 mm. This corresponds to an oxygen fractional absorption of 2.5×10^{-4} on the R11Q12 line at 760.445 nm (vacuum wavelength). Two identical photodiodes were used to detect the sample signal and the reference signal. In the left-hand part of Fig. 3a, the unprocessed sample signals together with the fitted reference signals are shown. The balanced-detection signals obtained according to (4) are shown in the right-hand part of the figure together with the fitted ideal experimental absorption profile. As can be seen in the figure, all components of $\boldsymbol{h}$ are needed to obtain a satisfactory balanced-detected signal. However, the influence of l_1 is very small, i.e. the non-linear amplification response compensation is not of great influence when using two identical detectors in our experimental setup.

The same procedure was carried out after changing the sample detector to a PMT. The reference signal was still recorded by a photodiode. The influence of the different $\boldsymbol{h}$-parameter combinations is shown in Fig. 3b. In this figure it can be observed that l_1 is of greater influence when employing detectors of different types to record the sample signal and the reference signal than when two identical detectors are used.

The observations in Fig. 3 and our general experience can be summarized in the following points:

- In the case with identical detectors it is sufficient to parameterize with fewer variables, while in the case of different types of detectors all parameters discussed are significant.
- In applications where the light intensity varies widely (large dynamic range) residual differences between similar detectors are more important and again call for more detailed parametrization. Thus, we retain all parameters for general purposes.

To compare the presented software-based method with the analog method [11], measurements with both approaches were performed with an air distance of about 6 mm (fractional

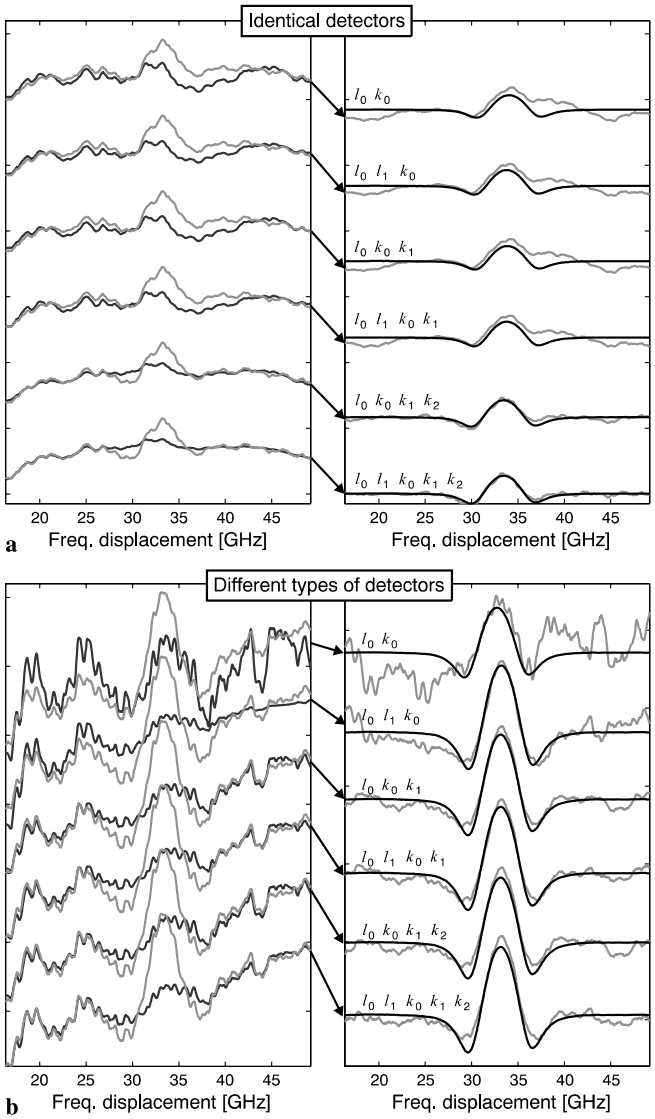

FIGURE 3 Typical curves obtained during software-based balanced detection with 10 mm of air distance. *To the left*: the *gray curves* show $\boldsymbol{p}_{\mathrm{samp}}$ and the *black curves* the fitted $\boldsymbol{p}_{\mathrm{ref}}$. *To the right*: the *gray curves* show the corresponding $\boldsymbol{p}_{\mathrm{bds}}$ and the *black curves* the fitted $\boldsymbol{p}_{\mathrm{i}}$. The influences of the different $\boldsymbol{h}$-parameter combinations are presented. (**a**) Two identical detectors have been used to detect the sample beam and the reference beam. (**b**) Two different types of detectors have been used to detect the sample signal and the reference signal

absorption of 1.5×10^{-4}). An attenuation filter was placed in front of the sample detector to provide a reference beam power 100 times the sample beam power ($P_{\mathrm{ref}}/P_{\mathrm{samp}}\approx100$). This was done to optimize the performance of the analog device. In Fig. 4a obtained balanced-detection signals from both methods are shown when using two identical detectors. The measured unprocessed sample signal is also included. It can be seen that when performing analog balanced detection a large offset remains. Attempts were made to compensate for this by adjusting the offset in the device, but no difference could be seen. An 'ideal' experimental absorption profile was fitted to the software-based balanced-detection signal. The global intensity parameter, i.e. the peak-to-peak value of the fitted ideal experimental absorption profile, was estimated to be 0.44 scale units. This corresponds to an air distance of

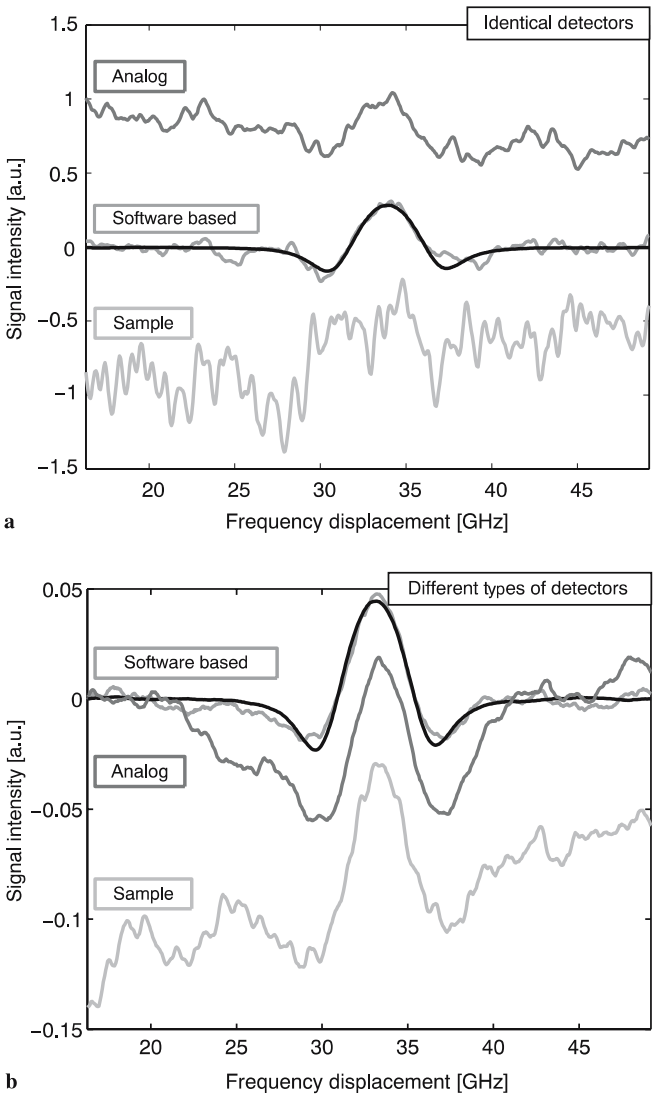

FIGURE 4 Achieved balanced-detection signals by using the software-based algorithm, $\boldsymbol{p}_{\mathrm{bds}}$, and the analog device. The unprocessed sample signal measured, $\boldsymbol{p}_{\mathrm{samp}}$, is also shown. No collimator package was used on the sample beam. (**a**) About 6 mm of added air distance. Two identical detectors were used to detect the sample signal and the reference signal ($P_{\mathrm{ref}}/P_{\mathrm{samp}} \approx 100$). (**b**) About 10 mm of added air distance. Two different types of detectors were used to detect the sample signal and the reference signal ($P_{\mathrm{ref}}/P_{\mathrm{samp}} \approx 4$). The curve with *darkest tone* is an 'ideal' experimental curve, $\boldsymbol{p}_{\mathrm{i}}$, fitted to the data

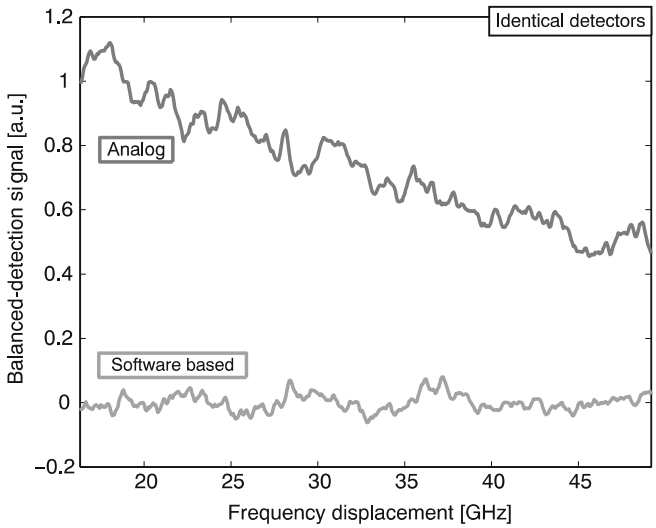

FIGURE 5 Achieved balanced-detection signals with no added air distance by using the software-based method, $\boldsymbol{p}_{\mathrm{bds}}$, and the analog device. Two identical detectors were used to detect the sample signal and the reference signal. No collimator package was used on the sample beam

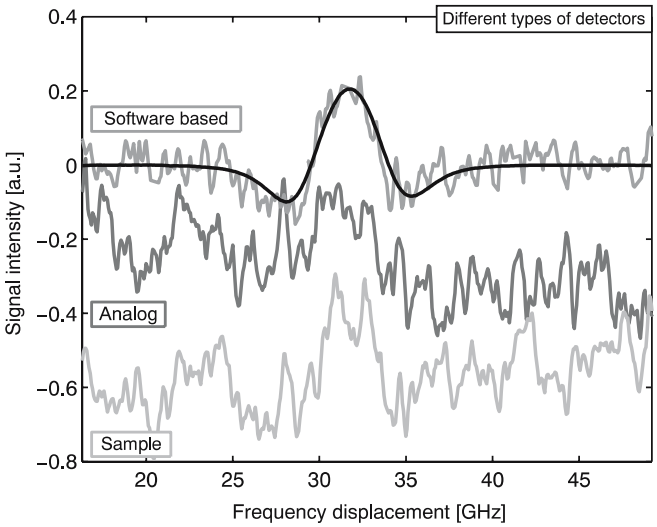

FIGURE 6 Achieved balanced-detection signals by using the software-based method, $\boldsymbol{p}_{\mathrm{bds}}$, and the analog device measured through the maxillary sinus on a human volunteer. The unprocessed sample signal measured, $\boldsymbol{p}_{\mathrm{samp}}$, is also shown. The curve with *darkest tone* is an 'ideal' experimental curve, $\boldsymbol{p}_{\mathrm{i}}$, fitted to the data

6.3 mm (calibration information is provided in Fig. 7 in the appendix).

Figure 4b shows signals obtained for a 10-mm air distance when using detectors of different types. The reference signal power was now only a factor of four larger than the sample signal power ($P_{\mathrm{ref}}/P_{\mathrm{samp}} \approx 4$). It can be seen that both methods are able to retrieve the oxygen signal; however, the software-based method is more successful. The peak-to-peak value of the fitted ideal experimental absorption profile was estimated to be 0.07 local scale units. This corresponds to an air distance of 10 mm. In Fig. 4a and b, an optical interference fringe reduction of about 10 times by the use of the algorithm approach can be seen compared to the sample signal. In the case of the analog method a baseline correction is needed, which would require a software approach. Then the full computational technique put forward in the present paper rather would come to mind.

To study the noise level remaining after performing balanced detection, and thereby the limitations of the experimental arrangement together with the algorithm, measurements were done with no air distance between the light source and the sample detector. Ideally, this should result in a zero signal, since the sample signal should not contain any oxygen imprint. Figure 5 shows the balanced-detection signals obtained with the software-based and the analog methods when using two identical detectors. In this figure it is again obvious that the analog noise reduction device does not fully compensate for offset differences between the sample signal and the reference signal. A noise level of about 0.15 scale units remains after the data are processed by the algorithm.

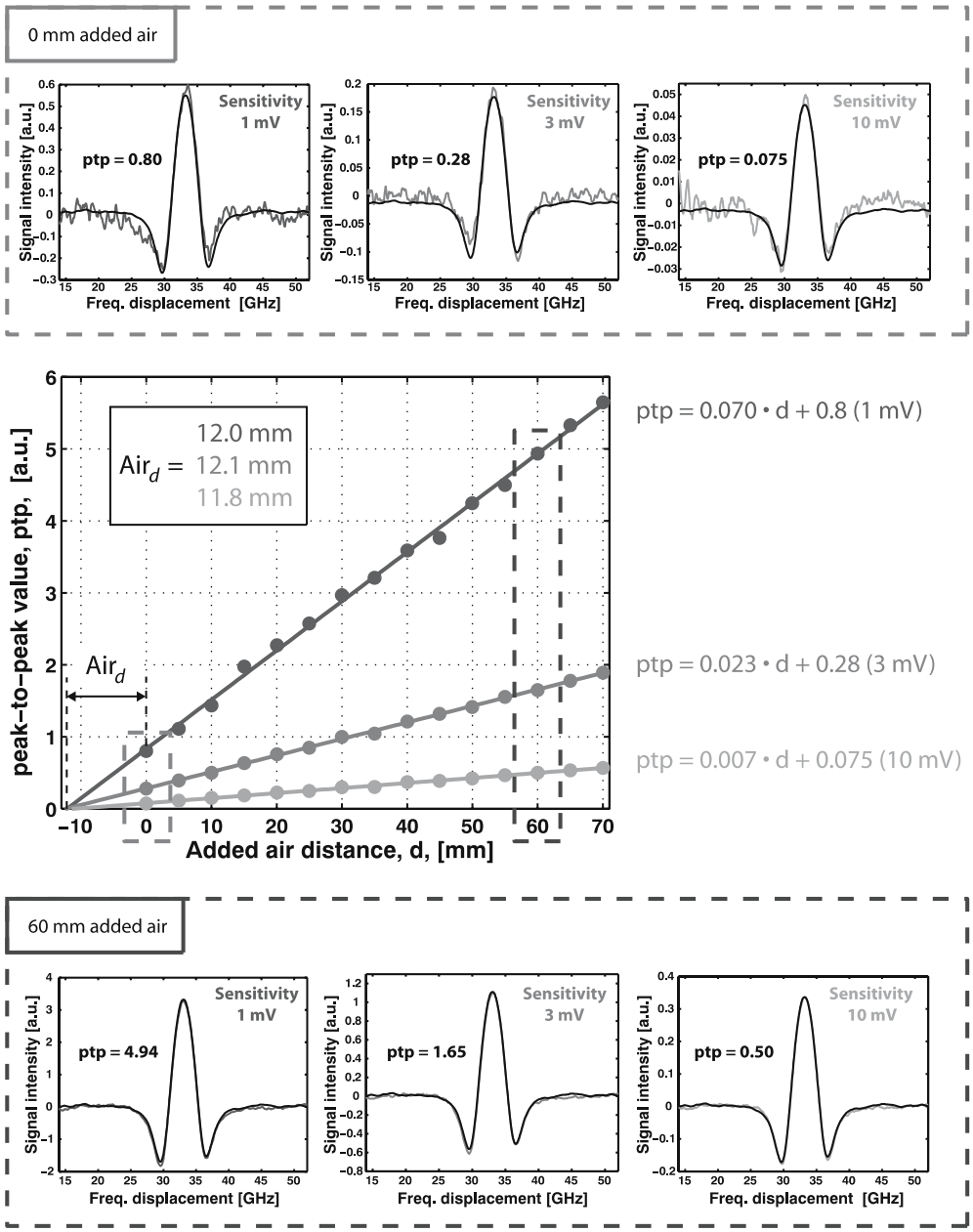

FIGURE 7 Results from measurements according to the standard addition method. Six obtained balanced-detection signals, p_{bds}, from 0 mm to 60 mm of added air distance measurements and the three different sensitivities used of the lock-in amplifier are included together with their estimated peak-to-peak values. The equations of the linear relationship between the peak-to-peak values and the added air distances for the three sensitivities are presented. The estimated unknown air distance, Air$_d$, of the collimator package was estimated to about 12 mm for all sensitivities

This corresponds to a signal of about 2 mm of air distance (a fractional absorption of 5×10^{-5}), which is a measure of the resolution of our experimental setup together with the algorithm.

As a final and most critical example we present data from a case where the sample is strongly scattering and attenuating. Here there is an unknown intensity relationship between the sample and the reference signals. Measurements on an air-filled human maxillary sinus cavity, located within the cranial skeleton below the orbital floor [19], are shown in Fig. 6. The fibre end is then placed inside the mouth on the palate and the multiply scattered light is detected externally on the cheekbone by a handheld probe containing the PMT. The achieved balanced-detection signal in the software-based approach corresponds to an air distance of about 10 mm. In the figure it can clearly be seen that a larger 'noise floor' of the balanced-detection signal remains in the analog approach compared to the software-based method even though correction of the baseline would be performed.

The calibration of the system is discussed in detail in the appendix.

5 Conclusion

In theory, intensity perturbations from laser and fibres, before the fibre coupler, should be canceled out by the analog noise cancellation device used in the study for comparison. However, due to detector channels' imperfections with regard to non-linearities and offsets, electronic cancellation of noise, based on the design described in Fig. 1b, is, in practice, imperfect. Figure 4 shows that the performance of the analog device was a factor of about two worse than achieved in the software-based approach as evaluated by comparing the remaining 'noise floor' in the absence of an absorption signal.

The new approach is, in contrast to the analog technique, forgiving in terms of signal levels, gain settings, and offsets, since the technique adjusts for all these factors. In particular, it was demonstrated (Fig. 3b) that quite different detectors can be used and still a very satisfactory balanced detection can be achieved. However, we note that two lock-in amplifiers were employed in the software-based method in contrast to only one in the analog approach. Since intensity drifts due to optical interference fringes can be expected to occur on a slow time scale, the use of one lock-in amplifier sequentially for recording the sample and the reference signals should be feasible. Then, signal averaging individually for the two signals could be performed as customarily done in, for example, differential absorption lidar (DIAL) [21].

Clearly, the techniques presented here only compensate for 'upstream' fringes generated in and close to the laser source, while differential fringe effects in the two detector paths remain untreated. This is also the case for the analog approach.

However, major sources of such differential fringe generation (e.g. absorption cells) are not present in most of our applications. Rather, we deal with cases of free-air propagation (long-path-absorption remote sensing) or gas pores or cavities embedded in scattering media [15–19].

Our experience shows that substantial and very valuable improved signals are observed in practical measurements. As already mentioned, the technique described is particularly useful when pigtailed lasers are employed and customary fringe elimination by shaking is not possible. Possible fringes between the two detectors can still be eliminated, for example by mechanical vibration.

ACKNOWLEDGEMENTS This research was supported by the Swedish Research Council, the Swedish Foundation for Strategic Research, and the Knut and Alice Wallenberg Foundation.

Appendix

Calibration measurements

The standard addition method (see e.g. [4]) was used in order to further investigate the algorithm presented, and to calibrate our measured signals and thereby be able to estimate the air distance from a recorded peak-to-peak value. The method is based on adding known path lengths of air and measuring the peak-to-peak value for each distance. The measured values are then plotted as a function of added air. These values should be linear with regard to the added air distance, since the absorption is so low that the fractional absorption is proportional to the concentration and the distance the light has traveled. A collimator package, described in Sect. 2, was placed on the fibre end of the sample part. Due to the design of the package, an unknown air distance was added between the fibre tip and the sample detector. The collimator package was moved away from the light source, in 5-mm steps, and the peak-to-peak values of the obtained processed signals were estimated for the different air distances. Three different sensitivities (1 mV, 3 mV, and 10 mV) of the lock-in amplifier were used at each added air distance. In Fig. 7 the results can be seen. In the figure, six obtained balanced-detection signals, from 0 mm to 60 mm of added air distances, are also shown together with their estimated peak-to-peak values. As can be seen, the values follow the expected linear relationship with regard to the added air distance. The slope of the curves was estimated and can then be used as a calibration factor (included in the figure). The relationship between the different sensitivities can also be seen. The peak-to-peak values from a fixed air distance for different sensitivities of the lock-in amplifier should scale with the sensitivity of the unit. Our estimated slopes of the curves agree with this to a high precision. The unknown air distance, Air_d, in the collimator package could be estimated to be about 12 mm. Measurements from all sensitivities gave approximately the same value (also included in the figure).

REFERENCES

1 M.W. Sigrist (ed.), *Air Monitoring by Spectroscopic Techniques* (Wiley, New York, 1994)
2 P. Werle, Spectrochim. Acta A **54**, 197 (1998)
3 E.I. Moses, C.L. Tang, Opt. Lett. **1**, 115 (1977)
4 S. Svanberg, *Atomic and Molecular Spectroscopy*, 4th edn. (Springer, Berlin, 2004)
5 P. Werle, R. Mücke, F. Slemr, Appl. Phys. B **57**, 131 (1993)
6 D.R. Hjelme, S. Neegård, E. Vartdal, Opt. Lett. **20**, 1731 (1995)
7 V. Liger, Spectrochim. Acta A **55**, 2021 (1999)
8 S. Wu, T. Kimishimai, Y. Yoshi, H. Kuze, N. Takeuch, Opt. Rev. **9**, 189 (2002)
9 P. Hobbs, Appl. Opt. **36**, 903 (1997)
10 V. Liger, A. Zybin, Y. Kuritsyn, K. Niemax, Spectrochim. Acta B **52**, 1125 (1997)
11 C. Lindsay, R. Rade, T. Oka, J. Mol. Spectrosc. **210**, 51 (2001)
12 X. Zhu, D.T. Cassidy, Appl. Opt. **34**, 8303 (1995)
13 R. Engelbrecht, Spectrochim. Acta A **60**, 3291 (2004)
14 P. Vogel, V. Ebert, Appl. Phys. B **72**, 127 (2001)
15 M. Sjöholm, G. Somesfalean, J. Alnis, S. Andersson-Engels, S. Svanberg, Opt. Lett. **26**, 16 (2001)
16 L. Persson, K. Svanberg, S. Svanberg, Appl. Phys. B **82**, 313 (2006)
17 M. Andersson, L. Persson, M. Sjöholm, S. Svanberg, Opt. Express **14**, 3641 (2006)
18 T. Svensson, L. Persson, M. Andersson, S. Andersson-Engels, S. Svanberg, J. Johansson, S. Folestad, Non-invasive characterization of pharmaceutical solids using diode laser oxygen spectroscopy, manuscript in preparation (2007)
19 L. Persson, M. Andersson, T. Svensson, K. Svanberg, S. Svanberg, Non-intrusive optical study of gas and its exchange in human maxillary sinuses, manuscript in preparation (2007)
20 R.A. Horn, C.R. Johnsson, *Topics in Matrix Analysis* (Cambridge University Press, New York, 1994)
21 S. Svanberg, Differential absorption lidar (DIAL), in *Air Monitoring by Spectroscopic Techniques*, ed. by M.W. Sigrist (Wiley, New York, 1994), Chap. 3